

Highlights

The seeding method: A test case for classical nucleation theory in small systems

Thomas Philippe, Yijian Wu, Aymane Graini

- We perform NVT seeded simulations of Lennard-Jones condensation in small systems to stabilize critical droplets and compare their properties with classical nucleation theory predictions.
- We demonstrate how the classical nucleation theory can guide the setup of NVT seeded simulations and concomitantly evaluate the existing thermodynamic models.

The seeding method: A test case for classical nucleation theory in small systems

Thomas Philippe^a, Yijian Wu^a, Aymane Graini^a

^a*Laboratoire de Physique de la Matière Condensée, Ecole polytechnique, CNRS, IP Paris, Palaiseau, 91128, France*

Abstract

Molecular dynamics simulations are widely used to investigate nucleation in first-order phase transitions. Brute-force simulations, though popular, are limited to conditions of high metastability, where the critical cluster and the nucleation barrier are small. The seeding method has recently emerged as a powerful alternative for exploring lower supersaturation regimes by initiating simulations with a pre-formed nucleus. In confined systems (NVT ensemble), the seeded simulations are particularly effective for determining stable cluster properties and provide a stringent test case for classical nucleation theory (CNT). In this work, we perform NVT seeded simulations of Lennard-Jones condensation in small systems and compare them with CNT predictions based on several thermodynamic models, including equations of state, perturbation theory, and ideal gas approximation. We find that CNT accurately predicts stable cluster radii across a wide range of conditions. Notably, even the very simple ideal gas approximation proves useful for initializing seeded simulations. Furthermore, seeded simulation results correspond to the critical cluster radii of infinite systems: CNT predictions with good equations of state show very good agreement with simulations, while the perturbation theory and the ideal gas approximation perform well at low temperatures but deviate significantly at high temperatures.

Keywords: classical nucleation theory, seeding approach, small systems, condensation, critical clusters

1. Introduction

Nucleation is a rare and thermally activated process. In molecular dynamics (MD) simulations, only small critical clusters with low nucleation

barrier — in the regime of high supersaturation — are accessible with brute-force approaches [1, 2, 3, 4, 5, 6, 7], even when the simulation system is large [8, 9, 10]. While nucleation rates can be readily measured from brute-force simulations [11, 1], identifying critical clusters remains highly challenging [12]. A common strategy to estimate the critical cluster size is to apply the nucleation theorem [13] from measured nucleation rate [8]. However, in the high-supersaturation regime, classical nucleation assumptions become questionable [7]. To overcome these limitations, a variety of rare-event simulation techniques have been developed to promote the formation of critical cluster [14, 15, 16, 17, 18, 19, 20, 21, 22, 23, 24, 25, 26, 27]. These methods are well suited for investigating nucleation with larger nucleation barriers and at lower supersaturation [28]. In parallel, another approach has emerged: the seeding technique [29, 30, 31, 32]. In seeded MD simulations, the system is initialized with a pre-formed nucleus of the new phase. At constant pressure and temperature (NPT ensemble), the inserted seed may either grow (if post-critical) or redissolve (if pre-critical). At the exact critical size, the cluster corresponds to an unstable equilibrium, with a 50% probability of growth or dissolution. Once the critical cluster is identified, classical nucleation theory (CNT) [13, 33, 34, 35, 36, 37, 38], on which the approach relies, can then be applied to estimate the nucleation rate [29]. This approach is conceptually simple and intuitive, but in practice requires many independent simulations to pinpoint the condition at which the seed is critical. Moreover, because the seeds typically grow or redissolve rapidly, NPT seeding can be computationally intensive when aiming for robust statistics.

In order to make the seeding technique more versatile, the method was then extended to the NVT ensemble [30, 31, 39, 40, 41]. This approach builds on the framework of classical nucleation in small systems [42, 43, 44, 45, 46, 47, 48]. Mass conservation, together with chemical and mechanical equilibrium conditions, give rise to two critical states: one unstable and the other stable [45]. The objective of NVT seeded simulations is to achieve the stable equilibrated configuration, which corresponds to the critical unstable cluster in the NPT ensemble or, equivalently, in the infinite system at the corresponding supersaturation [29, 41]. Yet, nucleation in confined systems is also known to present some peculiarities, such as superstabilization, and finite-size effects must be carefully accounted for when applying the NVT seeding approach.

In this paper, we apply CNT to study the condensation of nanodroplets in the NVT ensemble. Lennard-Jones particles are chosen as a model system,

and *a priori* for testing some thermodynamic models, since many efforts have been devoted to developing, for instance, accurate equation of states (EOS) for this system [49, 50, 51]. We demonstrate then how CNT can guide the setup of NVT seeded simulations and concomitantly evaluate the existing thermodynamic models. We first briefly describe the NVT seeding method for condensation of Lennard-Jones particles.

2. Simulation details

Simulations were performed using the open-source package **LAMMPS** [52, 53]. For the Lennard-Jones interactions, we used a large cutoff of 6.78σ with σ the length parameter [54, 55]. Lennard-Jones units are used in the following. Energies are scaled by ϵ , which is the energy depth of the untruncated Lennard-Jones potential. Lengths are scaled by σ , temperatures by ϵ/k_B , densities by σ^{-3} , and time by $\tau = \sqrt{m\sigma^2/\epsilon}$ with m the mass of the particle. The timestep employed is 0.005τ . Cubic periodic boundary conditions are used. For temperature control, we employed the Nose-Hoover thermostat implemented in **LAMMPS** with damping parameter taken as 0.5τ . We use the following procedure for performing seeded simulations. The first step is to prepare the seed. The seed is obtained from a NVT run in a box of arbitrary size to equilibrate the single phase liquid state at the density of the phase diagram $\bar{\rho}_l$, which sets the number of particles in the chosen volume. Then a sphere of a given size R is extracted from the liquid phase and inserted in a cubic box of size L . This sets the initial number of liquid particles, N_l , in the seeded simulation:

$$N_l = \frac{4}{3}\pi R^3 \bar{\rho}_l. \quad (1)$$

It remains to choose the initial number of vapor particles, N_v , which are randomly distributed outside the liquid droplet. The box density, ρ , is then given by:

$$\rho = \frac{N_l + N_v}{L^3}. \quad (2)$$

Therefore, for a given box size L , there are two independent parameters, R and ρ , that must be carefully chosen to guarantee that the subsequent NVT run leads to the stabilization of the liquid droplet to the expected (stable) equilibrium in the confined system. However, nucleation in small systems present some peculiarities, detailed in the following section, that can complicate the choice of the parameters of NVT seeded simulations.

For instance, if a given triplet (L, R, ρ) implies a too large value of the initial vapor density, spontaneous and undesired thermally activated nuclei will form in the vapor phase. The seed can also redissolve if the initial vapor density is too small. Moreover, for a given ρ , no stable cluster will exist if the box size L is too small, due to the so-called superstabilization effect [45]. As we will show in the following, the NVT-seeding approach can greatly benefit from insights of classical nucleation theory.

3. Classical nucleation theory

In an infinite system, a supersaturated vapor phase is initially metastable, i.e. the formation of the stable phase (liquid) is energetically favorable for sufficiently large clusters. Yet, in a confined (finite) system, both the size of the critical cluster and the nucleation barrier are known to increase as compared with nucleation in the infinite system. Therefore, the phase transition is systematically delayed. But as the size of the confined system decreases, nucleation can be impeded and the initial state is no more metastable but becomes stable, because of mass conservation [45]. Thus, for a given supersaturation this superstabilization effect can prevent nucleation to occur in too small systems. In larger systems however, generally, a new minimum in energy appears, associated with the formation of a nucleus that corresponds to a stable and final state, as growth is stopped. The calculation of this stable equilibrium is reminded in this section. Following many theoretical works dedicated to first-order phase transitions in confined systems [42, 43, 44, 45, 46, 47, 48, 56], we consider CNT in the NVT ensemble within the capillary approximation. N is the total number of particles in the system, $V = L^3$ its volume, and T the fixed temperature. The system therefore consists of a spherical liquid nucleus of radius R (with homogeneous density ρ_l) in the vapor phase of density ρ_v . In the capillary approximation, the liquid and vapor phases are separated by a sharp interface with constant surface tension γ .

In the NVT (canonical) ensemble, the appropriate thermodynamic potential to consider is the Helmholtz free energy, F . Since the cluster is spherical, the variation of the total Helmholtz free energy of the system is given by [45]

$$dF = \left(p_v - p_l + \frac{2\gamma}{R} \right) dV_l + (\mu_l - \mu_v) dN_l, \quad (3)$$

where p_l and p_v denote the liquid and vapor pressures, respectively, and

μ_l and μ_v denote the chemical potentials of the liquid and vapor phases, respectively. V_l is the volume of the droplet of radius R , which contains N_l particles. At equilibrium, $dF = 0$, leading to the equality of the chemical potentials of the liquid and vapor phases,

$$\mu_l^* = \mu_v^*, \quad (4)$$

and the Laplace relation

$$p_l^* - p_v^* = \frac{2\gamma}{R^*}. \quad (5)$$

Properties marked with * are those at equilibrium. In an infinite system, or when the chemical potential of the vapor phase is fixed and known (in the grand canonical ensemble for instance), supersaturation is fixed and the above system admits only one solution that corresponds to the unstable equilibrium and sets the properties of the critical cluster, namely its density ρ^* and its size R^* . However, in the canonical ensemble, the total number of particles (i.e., mass) is conserved, the vapor phase density is not fixed but depends on the number of molecules constituting the droplet,

$$\rho = \Phi \rho_l + (1 - \Phi) \rho_v, \quad (6)$$

where $\Phi = V_l/V$ is the volume fraction occupied by the liquid. The critical droplet must also satisfy the above condition. The combination of mass conservation and the equilibrium conditions has now two solutions, one corresponding to the critical and unstable cluster, and the other corresponding to a larger and stable droplet in equilibrium with the vapor. The size of the unstable critical cluster is known to slightly increase in a confined system [46], as compared with that in the infinite system, which delays the phase transition. An approximated expression for the critical droplet in small systems can be obtained from expanding the pressures and densities at first order [47]. The larger droplet corresponds to a stable equilibrium. The objective of seeded simulations in the NVT ensemble is to equilibrate this droplet in the vapor phase.

In practice, the critical densities of both the stable and unstable clusters are very close to that of the phase diagram, $\bar{\rho}_l$. If we further assume that the vapor phase is ideal and the liquid phase incompressible, one gets the usual relation for both critical sizes,

$$R^* = \frac{2\gamma}{\bar{\rho}_l T \ln S^*}, \quad (7)$$

in reduced units, with $S^* = p_v^*/\bar{p}_v$ the ratio between the vapor pressure at equilibrium and that of the saturated vapor. Since the vapor is assumed to be ideal gas, $S^* = \rho_v^*/\bar{\rho}_v$, where $\bar{\rho}_v$ is the saturated vapor density of the phase diagram. Together with Eq. (6) and $\rho_l^* = \bar{\rho}_l$, Eq. (7) constitutes the approximate problem derived by Reguera et al. [45] to find both the unstable and stable clusters in confined systems. However, if quantitative predictions are intended, a more rigorous thermodynamic description of the chemical potential should be required, as we shall see.

4. Results

We investigate the condensation of Lennard-Jones particles over the temperature range from 0.7 to 1.1. The two solutions of Eqs. (4), (5), and (6) are obtained using chemical potential computed from the EOS developed by Johnson, Zollweg, and Gubbins (JZG) [49]. The EOS are combined with a mean-field correction for the cut potential [49], using the same cutoff (6.78) as in the simulations. Within this temperature range, the phase diagram predicted by the JZG EOS is found to be in excellent agreement with that obtained from MD simulations of the two-phase system at equilibrium (not shown). The surface tension of the planar vapor/liquid interface at equilibrium is classically calculated from MD simulations using the Kirkwood pressure tensor method [57]. The results follow the expected power law [55], $\gamma = \gamma_0 (1 - T/T_c)^a$, with $\gamma_0 = 2.838$, $a = 1.252$, and $T_c = 1.305$ the critical temperature.

Fig. 1(a) presents the two solution branches as a function of box density ρ at $T = 0.7$ for various box sizes, $L = 30$ (red), 50 (blue), and 70 (orange), obtained using the JZG EOS and the computed surface tension. The smaller droplet (dashed lines) corresponds to the unstable equilibrium, while the larger droplet (solid lines) represents the stable cluster. As expected [45, 47, 48], the two branches merge for the density at which the superstabilization effect operates, i.e., no cluster forms since the vapor phase at this given box density becomes stable. For supersaturation between the binodal limit (vertical black dotted line) and this box density, nucleation is therefore impeded [45]. Predictions obtained from the approximate relations, Eq. (6) with $\rho_l^* = \bar{\rho}_l$ and Eq. (7), are also shown: stable and unstable branches are represented by dash-dotted and dotted lines, respectively. They agree very well with the JZG EOS results, particularly for the upper branches corresponding to the stable clusters.

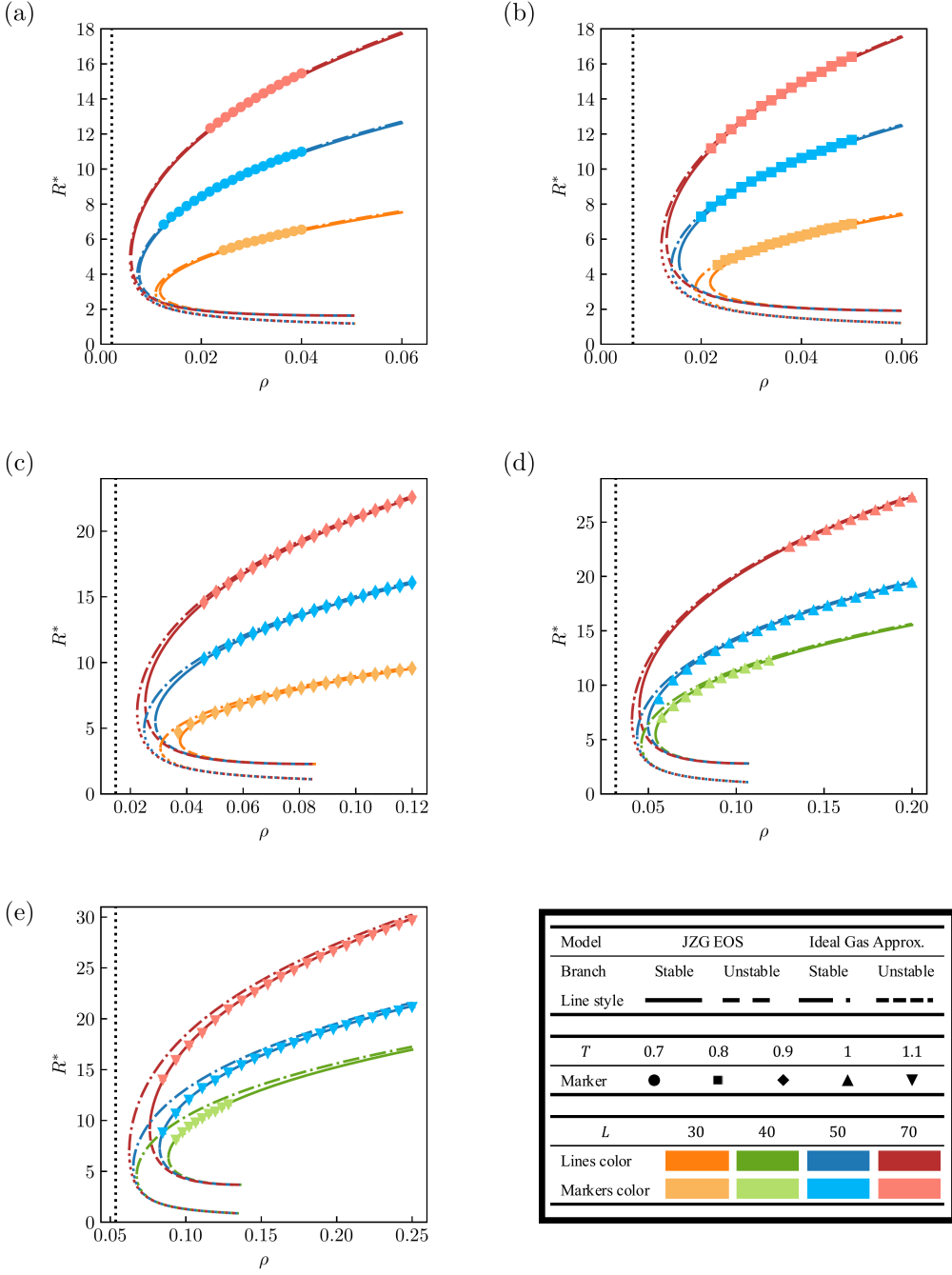


Figure 1: Evolution of critical radius against box density of confined system with different box sizes and at different temperatures: (a) $T = 0.7$, (b) $T = 0.8$, (c) $T = 0.9$, (d) $T = 1$, and (e) $T = 1.1$. Legends are in the bottom right. Color lines represent predictions and markers represent MD results. Vertical dotted black lines indicate the binodal limit for each temperature.

The seeding technique is then employed to find the stable clusters at this temperature. For each box size, a single simulation run is performed. For example, in the case $L = 70$ a liquid seed of density $\bar{\rho}_l$ is introduced with an initial radius R chosen very close to the theoretical predictions for the highest box density $\rho = 0.04$. Mass conservation then determines the vapor density of the initial state. An NVT simulation is run for a sufficiently long time (typically 5000 to 10000 τ) to equilibrate the liquid cluster with the vapor. Equilibration is very fast, since the initial seed is prepared near the targeted cluster. The radius of the stable cluster, R^* , for this box size and density is averaged over the last 100 stable configurations (dumped every 5τ). To explore a lower box density, vapor particles are randomly removed, after which a new NVT run is carried out to equilibrate the cluster. This process is repeated iteratively to obtain stable liquid clusters at a range of box densities. The key advantage of this procedure is that the initial seed is always prepared close to the stable cluster, resulting in very efficient seeding simulations.

In order to measure the cluster properties, we use **Ovito** [58] and first segment the liquid droplet by clustering analysis. A clustering distance, d , is defined, and particles forming a connected set — each within a distance d of at least one other — are identified; the number of such particles are denoted n^* . The clustering analysis is not very sensitive to d within the conventional range [1.2, 1.5] for Lennard-Jones droplets [8]; in our analysis we adopt $d = 1.25$. Several methods available in **Ovito**'s MD standard analysis library can then be used to determine the cluster radius: (i) fitting the radial density profile, or its integral, in simulation to a modified sigmoidal function [9, 59], (ii) the convex hull method [58], or (iii) the radius of gyration [58]. The radius may also be estimated from the droplet volume, $R^* = (3n^*/(4\pi\bar{\rho}_l))^{1/3}$, assuming the droplet is homogeneous with bulk liquid density $\bar{\rho}_l$ from the phase diagram. In our case, all methods yield very similar results, since the clusters are well defined, nearly spherical, and relatively large. For sake of clarity, only the results obtained from the droplet volume estimation are shown. The corresponding results are also shown in Fig. 1(a) as light-colored circles with error bars. The error bars, representing standard deviations in R^* , are too small to be visible. With three configurations ($L = 30$, 50, and 70), stable clusters with radius ranging from 5 to 16 are obtained. Remarkably, the seeding results are reproduced very well by CNT predictions using either the JZG EOS or the ideal gas approximation. Fig. 1(b)-(e) present seeded simulation results at higher temperatures: $T = 0.8$, $T = 0.9$, $T = 1$,

and $T = 1.1$. Agreement with CNT predictions using the JZG EOS remains excellent across this range. In contrast, the ideal gas approximation becomes unreliable at high temperature. Nevertheless, it provides sufficiently accurate estimates to serve as practical initial conditions for seeded simulations, owing to the simplicity of the corresponding CNT calculations.

As mentioned earlier, the purpose of seeded simulations in the NVT ensemble is to achieve the equilibrated configuration corresponding to a stable cluster, characterized by radius R^* and density ρ_l^* , in equilibrium with a vapor phase of density ρ_v^* . The same cluster, in fact, is unstable in the NPT and μ PT ensembles, as well as in infinite systems at vapor density ρ_v^* [41, 47]. In these cases, the cluster still satisfies the equilibrium conditions, Eqs. (4) and (5), but under conditions of fixed supersaturation. Nucleation is frequently studied under such circumstances, where either the pressure or the chemical potential of the surrounding phase is imposed. The equilibrium vapor density of a seeded simulation is estimated by $\rho_l^* = (N - n^*) / (V - 4\pi R^{*3}/3)$. The evolutions of critical cluster radius against vapor density at different temperatures are presented in Fig. 2 by light-colored markers with error bars. The legend for markers is identical to that in Fig. 1. The error bars represent standard deviations in ρ_v^* and R^* , while the latter is invisible in the figure. At each temperature, the expected dependence of cluster size on supersaturation is recovered: the critical radius diverges as the vapor density approaches the binodal limit. As expected, fluctuations tend to increase with temperature and are more pronounced for smaller box sizes, primarily due to fluctuation in radius having a more substantial impact on vapor. CNT predictions by Eqs. (4) and (5) at fixed ρ_v^* are also reported as black lines. Several thermodynamic models are employed to compute the chemical potential: the JZG EOS as previously, the Kolafa and Nezbeda (KN) EOS [50], classical density functional theory (DFT) with perturbation theory [60], and the ideal gas approximation for the vapor phase [45] as Eq. (7). This constitutes a stringent test of the accuracy of these models, since CNT is expected to provide reliable predictions at low supersaturation, the regime relevant for the seeding technique. Overall, CNT predictions obtained with the JZG EOS show very good agreement with MD seeded simulations across the entire temperature range studied. The KN EOS also performs relatively well, especially at low temperature. Predictions based on DFT are accurate at low temperature but not so good at higher temperature, reflecting the limitations of DFT in describing bulk properties in this regime [61]. The ideal gas approximation also breaks down at high temperature, indicating that this approach should

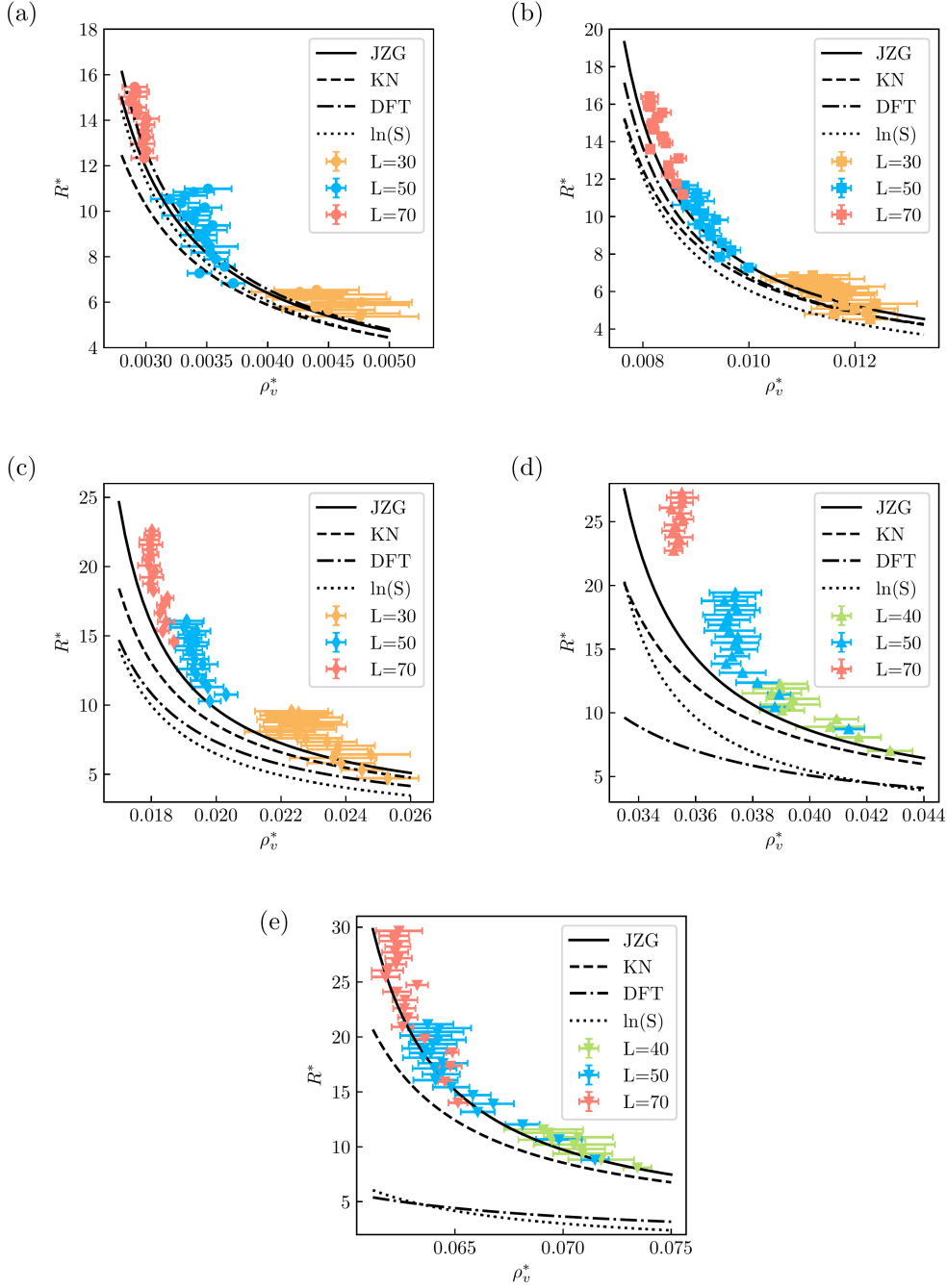


Figure 2: Evolution of critical radius against vapor density at different temperatures: (a) $T = 0.7$, (b) $T = 0.8$, (c) $T = 0.9$, (d) $T = 1$, and (e) $T = 1.1$. Markers represent measurements from seeded MD simulations of confined system, and their error bars represent standard deviations in ρ_v^* and R^* . Black lines represent CNT predictions with different thermodynamic models.

be employed with considerable caution.

5. Summary

The seeding technique has been applied to investigate the condensation of Lennard-Jones particles and, at the same time, to test both CNT and the accuracy of widely used thermodynamic models for Lennard-Jones fluid. The properties of the critical clusters predicted by CNT are found to agree well with seeded simulation results when JZG EOS is employed. The KN EOS also performs relatively well. In contrast, caution is required when using DFT or the ideal gas approximation, as both exhibit significant inaccuracies at high temperatures ($T \geq 0.9$). Nevertheless, the ideal gas approximation in confined systems, as expressed in Eqs. (6) and (7), remains of very practical value. It provides a simple and effective framework for initializing and guiding NVT seeded simulations, especially when no thermodynamic model for chemical potential is available.

Acknowledgments

This work was supported by the ANR TITANS project.

Appendix A. Simulation data

Table A.1 summarizes the results of our seeded MD simulations. Here, T denotes the temperature, L the box size, and ρ the box density. The stable cluster radius, R^* , and the corresponding vapor density, ρ_v^* are reported together with their standard deviations.

Table A.1: Our seeded MD simulation data. All data are in reduced units.

T	L	ρ	R^*	ρ_v^*
0.7	30	0.0244	5.369 ± 0.043	0.00475 ± 0.00048
0.7	30	0.0260	5.506 ± 0.027	0.00477 ± 0.00032
0.7	30	0.0276	5.659 ± 0.030	0.00450 ± 0.00038
0.7	30	0.0291	5.792 ± 0.025	0.00439 ± 0.00033

Continued on next page

T	L	ρ	R^*	ρ_v^*
0.7	30	0.0307	5.889 ± 0.035	0.00468 ± 0.00048
0.7	30	0.0322	5.998 ± 0.029	0.00477 ± 0.00041
0.7	30	0.0338	6.126 ± 0.032	0.00452 ± 0.00048
0.7	30	0.0353	6.247 ± 0.021	0.00430 ± 0.00032
0.7	30	0.0369	6.335 ± 0.027	0.00454 ± 0.00043
0.7	30	0.0384	6.452 ± 0.024	0.00426 ± 0.00039
0.7	30	0.0400	6.540 ± 0.020	0.00440 ± 0.00035
0.7	50	0.0125	6.834 ± 0.024	0.00372 ± 0.00009
0.7	50	0.0140	7.273 ± 0.022	0.00344 ± 0.00010
0.7	50	0.0156	7.564 ± 0.018	0.00365 ± 0.00008
0.7	50	0.0171	7.888 ± 0.019	0.00358 ± 0.00010
0.7	50	0.0186	8.184 ± 0.028	0.00353 ± 0.00016
0.7	50	0.0201	8.452 ± 0.038	0.00352 ± 0.00023
0.7	50	0.0217	8.709 ± 0.014	0.00349 ± 0.00009
0.7	50	0.0232	8.955 ± 0.022	0.00343 ± 0.00015
0.7	50	0.0247	9.171 ± 0.024	0.00350 ± 0.00017
0.7	50	0.0262	9.379 ± 0.019	0.00355 ± 0.00014
0.7	50	0.0278	9.605 ± 0.016	0.00340 ± 0.00013
0.7	50	0.0293	9.809 ± 0.024	0.00333 ± 0.00020
0.7	50	0.0308	9.988 ± 0.015	0.00341 ± 0.00013
0.7	50	0.0324	10.162 ± 0.016	0.00348 ± 0.00014
0.7	50	0.0339	10.360 ± 0.017	0.00329 ± 0.00015
0.7	50	0.0354	10.539 ± 0.016	0.00320 ± 0.00016
0.7	50	0.0369	10.691 ± 0.019	0.00332 ± 0.00018
0.7	50	0.0385	10.843 ± 0.017	0.00339 ± 0.00017
0.7	50	0.0400	10.987 ± 0.018	0.00351 ± 0.00019
0.7	70	0.0218	12.333 ± 0.023	0.00299 ± 0.00011
0.7	70	0.0233	12.652 ± 0.012	0.00300 ± 0.00006
0.7	70	0.0248	12.965 ± 0.019	0.00297 ± 0.00010
0.7	70	0.0264	13.253 ± 0.011	0.00300 ± 0.00006
0.7	70	0.0279	13.536 ± 0.010	0.00299 ± 0.00006
0.7	70	0.0294	13.804 ± 0.012	0.00300 ± 0.00007
0.7	70	0.0309	14.063 ± 0.017	0.00300 ± 0.00011
0.7	70	0.0324	14.324 ± 0.014	0.00293 ± 0.00009

Continued on next page

T	L	ρ	R^*	ρ_v^*
0.7	70	0.0339	14.566 ± 0.011	0.00293 ± 0.00007
0.7	70	0.0355	14.808 ± 0.011	0.00287 ± 0.00008
0.7	70	0.0370	15.031 ± 0.016	0.00289 ± 0.00011
0.7	70	0.0385	15.246 ± 0.014	0.00293 ± 0.00010
0.7	70	0.0400	15.462 ± 0.014	0.00291 ± 0.00010
0.8	30	0.0233	4.516 ± 0.069	0.01229 ± 0.00051
0.8	30	0.0248	4.792 ± 0.067	0.01161 ± 0.00056
0.8	30	0.0263	4.896 ± 0.060	0.01223 ± 0.00053
0.8	30	0.0278	5.086 ± 0.086	0.01199 ± 0.00082
0.8	30	0.0293	5.262 ± 0.049	0.01179 ± 0.00050
0.8	30	0.0307	5.349 ± 0.074	0.01239 ± 0.00078
0.8	30	0.0322	5.544 ± 0.046	0.01178 ± 0.00052
0.8	30	0.0337	5.701 ± 0.039	0.01147 ± 0.00047
0.8	30	0.0352	5.804 ± 0.051	0.01173 ± 0.00064
0.8	30	0.0367	5.926 ± 0.055	0.01170 ± 0.00072
0.8	30	0.0381	6.058 ± 0.039	0.01148 ± 0.00054
0.8	30	0.0396	6.166 ± 0.053	0.01151 ± 0.00075
0.8	30	0.0411	6.259 ± 0.059	0.01170 ± 0.00087
0.8	30	0.0426	6.390 ± 0.040	0.01129 ± 0.00061
0.8	30	0.0441	6.511 ± 0.034	0.01094 ± 0.00054
0.8	30	0.0456	6.601 ± 0.043	0.01102 ± 0.00070
0.8	30	0.0470	6.667 ± 0.041	0.01149 ± 0.00069
0.8	30	0.0485	6.795 ± 0.036	0.01085 ± 0.00062
0.8	30	0.0500	6.863 ± 0.039	0.01121 ± 0.00069
0.8	50	0.0200	7.277 ± 0.033	0.00999 ± 0.00014
0.8	50	0.0220	7.847 ± 0.039	0.00945 ± 0.00019
0.8	50	0.0240	8.203 ± 0.033	0.00967 ± 0.00018
0.8	50	0.0260	8.598 ± 0.029	0.00949 ± 0.00017
0.8	50	0.0280	8.964 ± 0.031	0.00928 ± 0.00020
0.8	50	0.0300	9.276 ± 0.028	0.00926 ± 0.00019
0.8	50	0.0320	9.592 ± 0.027	0.00906 ± 0.00020
0.8	50	0.0340	9.823 ± 0.030	0.00938 ± 0.00023
0.8	50	0.0360	10.110 ± 0.026	0.00914 ± 0.00021
0.8	50	0.0380	10.372 ± 0.027	0.00900 ± 0.00024

Continued on next page

T	L	ρ	R^*	ρ_v^*
0.8	50	0.0400	10.625 ± 0.027	0.00881 ± 0.00025
0.8	50	0.0420	10.822 ± 0.030	0.00906 ± 0.00029
0.8	50	0.0440	11.043 ± 0.023	0.00900 ± 0.00023
0.8	50	0.0460	11.247 ± 0.023	0.00902 ± 0.00024
0.8	50	0.0480	11.467 ± 0.022	0.00879 ± 0.00024
0.8	50	0.0500	11.660 ± 0.023	0.00878 ± 0.00025
0.8	70	0.0220	11.182 ± 0.029	0.00875 ± 0.00010
0.8	70	0.0240	11.748 ± 0.025	0.00863 ± 0.00010
0.8	70	0.0260	12.266 ± 0.034	0.00850 ± 0.00015
0.8	70	0.0280	12.722 ± 0.015	0.00848 ± 0.00007
0.8	70	0.0300	13.104 ± 0.029	0.00867 ± 0.00015
0.8	70	0.0320	13.601 ± 0.015	0.00814 ± 0.00008
0.8	70	0.0340	13.920 ± 0.022	0.00843 ± 0.00013
0.8	70	0.0360	14.283 ± 0.017	0.00838 ± 0.00010
0.8	70	0.0380	14.647 ± 0.015	0.00820 ± 0.00010
0.8	70	0.0400	14.971 ± 0.016	0.00818 ± 0.00010
0.8	70	0.0420	15.264 ± 0.014	0.00828 ± 0.00010
0.8	70	0.0440	15.548 ± 0.023	0.00836 ± 0.00017
0.8	70	0.0460	15.866 ± 0.015	0.00812 ± 0.00011
0.8	70	0.0480	16.138 ± 0.018	0.00814 ± 0.00014
0.8	70	0.0500	16.405 ± 0.020	0.00813 ± 0.00016
0.9	30	0.0370	4.711 ± 0.127	0.02529 ± 0.00095
0.9	30	0.0413	5.324 ± 0.066	0.02450 ± 0.00064
0.9	30	0.0457	5.806 ± 0.089	0.02385 ± 0.00104
0.9	30	0.0501	6.187 ± 0.101	0.02361 ± 0.00134
0.9	30	0.0544	6.432 ± 0.084	0.02477 ± 0.00121
0.9	30	0.0588	6.798 ± 0.057	0.02375 ± 0.00093
0.9	30	0.0632	7.068 ± 0.064	0.02376 ± 0.00114
0.9	30	0.0676	7.338 ± 0.047	0.02343 ± 0.00091
0.9	30	0.0719	7.605 ± 0.054	0.02277 ± 0.00112
0.9	30	0.0763	7.836 ± 0.043	0.02249 ± 0.00095
0.9	30	0.0807	8.065 ± 0.046	0.02197 ± 0.00109
0.9	30	0.0850	8.235 ± 0.045	0.02259 ± 0.00111
0.9	30	0.0894	8.427 ± 0.044	0.02249 ± 0.00114

Continued on next page

T	L	ρ	R^*	ρ_v^*
0.9	30	0.0938	8.589 ± 0.038	0.02298 ± 0.00105
0.9	30	0.0981	8.773 ± 0.042	0.02266 ± 0.00120
0.9	30	0.1025	8.954 ± 0.031	0.02221 ± 0.00095
0.9	30	0.1069	9.098 ± 0.037	0.02272 ± 0.00117
0.9	30	0.1113	9.262 ± 0.032	0.02240 ± 0.00105
0.9	30	0.1156	9.408 ± 0.031	0.02255 ± 0.00104
0.9	30	0.1200	9.559 ± 0.032	0.02232 ± 0.00113
0.9	50	0.0462	10.282 ± 0.043	0.01980 ± 0.00034
0.9	50	0.0505	10.761 ± 0.041	0.02031 ± 0.00036
0.9	50	0.0548	11.313 ± 0.050	0.01974 ± 0.00049
0.9	50	0.0592	11.776 ± 0.036	0.01959 ± 0.00039
0.9	50	0.0635	12.209 ± 0.026	0.01939 ± 0.00030
0.9	50	0.0679	12.605 ± 0.040	0.01929 ± 0.00050
0.9	50	0.0722	12.948 ± 0.035	0.01958 ± 0.00046
0.9	50	0.0766	13.312 ± 0.031	0.01933 ± 0.00043
0.9	50	0.0809	13.643 ± 0.022	0.01931 ± 0.00032
0.9	50	0.0852	13.966 ± 0.027	0.01916 ± 0.00041
0.9	50	0.0896	14.263 ± 0.031	0.01921 ± 0.00051
0.9	50	0.0939	14.540 ± 0.022	0.01939 ± 0.00038
0.9	50	0.0983	14.831 ± 0.024	0.01912 ± 0.00043
0.9	50	0.1026	15.091 ± 0.022	0.01925 ± 0.00042
0.9	50	0.1070	15.341 ± 0.022	0.01940 ± 0.00042
0.9	50	0.1113	15.610 ± 0.020	0.01901 ± 0.00041
0.9	50	0.1157	15.848 ± 0.024	0.01907 ± 0.00050
0.9	50	0.1200	16.081 ± 0.024	0.01909 ± 0.00052
0.9	70	0.0461	14.578 ± 0.024	0.01869 ± 0.00014
0.9	70	0.0504	15.364 ± 0.029	0.01835 ± 0.00019
0.9	70	0.0548	16.014 ± 0.036	0.01845 ± 0.00026
0.9	70	0.0591	16.652 ± 0.022	0.01826 ± 0.00017
0.9	70	0.0635	17.211 ± 0.023	0.01836 ± 0.00019
0.9	70	0.0678	17.732 ± 0.021	0.01850 ± 0.00019
0.9	70	0.0722	18.283 ± 0.017	0.01806 ± 0.00017
0.9	70	0.0765	18.770 ± 0.022	0.01796 ± 0.00022
0.9	70	0.0809	19.219 ± 0.033	0.01801 ± 0.00036

Continued on next page

T	L	ρ	R^*	ρ_v^*
0.9	70	0.0852	19.643 ± 0.018	0.01811 ± 0.00020
0.9	70	0.0896	20.074 ± 0.029	0.01792 ± 0.00034
0.9	70	0.0939	20.475 ± 0.014	0.01790 ± 0.00018
0.9	70	0.0983	20.851 ± 0.018	0.01799 ± 0.00023
0.9	70	0.1026	21.223 ± 0.016	0.01795 ± 0.00022
0.9	70	0.1070	21.578 ± 0.025	0.01798 ± 0.00036
0.9	70	0.1113	21.927 ± 0.021	0.01793 ± 0.00031
0.9	70	0.1157	22.257 ± 0.016	0.01802 ± 0.00024
0.9	70	0.1200	22.582 ± 0.013	0.01802 ± 0.00020
1.0	40	0.0576	7.006 ± 0.121	0.04281 ± 0.00078
1.0	40	0.0644	8.075 ± 0.090	0.04172 ± 0.00078
1.0	40	0.0712	8.905 ± 0.112	0.04072 ± 0.00120
1.0	40	0.0779	9.506 ± 0.062	0.04094 ± 0.00077
1.0	40	0.0847	10.189 ± 0.054	0.03903 ± 0.00078
1.0	40	0.0915	10.652 ± 0.065	0.03932 ± 0.00104
1.0	40	0.0983	11.089 ± 0.053	0.03941 ± 0.00093
1.0	40	0.1051	11.539 ± 0.054	0.03867 ± 0.00103
1.0	40	0.1118	11.903 ± 0.047	0.03899 ± 0.00097
1.0	40	0.1186	12.263 ± 0.043	0.03897 ± 0.00095
1.0	50	0.0560	8.722 ± 0.107	0.04137 ± 0.00055
1.0	50	0.0640	10.446 ± 0.068	0.03878 ± 0.00051
1.0	50	0.0720	11.434 ± 0.044	0.03893 ± 0.00040
1.0	50	0.0800	12.362 ± 0.069	0.03817 ± 0.00075
1.0	50	0.0880	13.146 ± 0.065	0.03765 ± 0.00081
1.0	50	0.0960	13.850 ± 0.037	0.03707 ± 0.00052
1.0	50	0.1040	14.437 ± 0.039	0.03728 ± 0.00060
1.0	50	0.1120	14.978 ± 0.039	0.03752 ± 0.00065
1.0	50	0.1200	15.503 ± 0.045	0.03739 ± 0.00083
1.0	50	0.1280	15.984 ± 0.040	0.03748 ± 0.00080
1.0	50	0.1360	16.455 ± 0.042	0.03719 ± 0.00088
1.0	50	0.1440	16.897 ± 0.024	0.03699 ± 0.00055
1.0	50	0.1520	17.302 ± 0.033	0.03712 ± 0.00079
1.0	50	0.1600	17.693 ± 0.035	0.03716 ± 0.00090
1.0	50	0.1680	18.058 ± 0.029	0.03746 ± 0.00079

Continued on next page

T	L	ρ	R^*	ρ_v^*
1.0	50	0.1760	18.423 ± 0.025	0.03738 ± 0.00072
1.0	50	0.1840	18.783 ± 0.027	0.03701 ± 0.00080
1.0	50	0.1920	19.107 ± 0.023	0.03736 ± 0.00073
1.0	50	0.2000	19.429 ± 0.027	0.03739 ± 0.00091
1.0	70	0.1304	22.732 ± 0.021	0.03523 ± 0.00031
1.0	70	0.1374	23.262 ± 0.021	0.03539 ± 0.00032
1.0	70	0.1444	23.778 ± 0.029	0.03541 ± 0.00048
1.0	70	0.1513	24.285 ± 0.023	0.03522 ± 0.00040
1.0	70	0.1583	24.756 ± 0.021	0.03529 ± 0.00039
1.0	70	0.1652	25.200 ± 0.018	0.03557 ± 0.00035
1.0	70	0.1722	25.649 ± 0.020	0.03545 ± 0.00039
1.0	70	0.1791	26.091 ± 0.019	0.03514 ± 0.00041
1.0	70	0.1861	26.488 ± 0.018	0.03552 ± 0.00039
1.0	70	0.1930	26.889 ± 0.024	0.03554 ± 0.00055
1.0	70	0.2000	27.280 ± 0.016	0.03552 ± 0.00038
1.1	40	0.0935	8.100 ± 0.083	0.07344 ± 0.00065
1.1	40	0.0979	8.829 ± 0.164	0.07176 ± 0.00152
1.1	40	0.1022	9.377 ± 0.130	0.07091 ± 0.00137
1.1	40	0.1066	9.795 ± 0.091	0.07088 ± 0.00106
1.1	40	0.1109	10.204 ± 0.148	0.07052 ± 0.00187
1.1	40	0.1153	10.634 ± 0.110	0.06948 ± 0.00155
1.1	40	0.1196	10.878 ± 0.109	0.07071 ± 0.00160
1.1	40	0.1239	11.276 ± 0.078	0.06936 ± 0.00125
1.1	40	0.1283	11.582 ± 0.107	0.06910 ± 0.00183
1.1	50	0.0848	8.813 ± 0.136	0.07148 ± 0.00063
1.1	50	0.0935	10.670 ± 0.152	0.06981 ± 0.00106
1.1	50	0.1022	12.034 ± 0.087	0.06813 ± 0.00079
1.1	50	0.1109	13.174 ± 0.071	0.06605 ± 0.00079
1.1	50	0.1196	13.919 ± 0.077	0.06677 ± 0.00096
1.1	50	0.1283	14.712 ± 0.058	0.06583 ± 0.00083
1.1	50	0.1370	15.429 ± 0.053	0.06483 ± 0.00084
1.1	50	0.1456	16.067 ± 0.058	0.06410 ± 0.00102
1.1	50	0.1543	16.605 ± 0.045	0.06436 ± 0.00086
1.1	50	0.1630	17.138 ± 0.049	0.06405 ± 0.00101

Continued on next page

T	L	ρ	R^*	ρ_v^*
1.1	50	0.1717	17.609 ± 0.051	0.06444 ± 0.00114
1.1	50	0.1804	18.110 ± 0.039	0.06353 ± 0.00094
1.1	50	0.1891	18.535 ± 0.038	0.06389 ± 0.00099
1.1	50	0.1978	18.965 ± 0.038	0.06360 ± 0.00104
1.1	50	0.2065	19.353 ± 0.038	0.06397 ± 0.00111
1.1	50	0.2152	19.730 ± 0.041	0.06423 ± 0.00128
1.1	50	0.2239	20.120 ± 0.036	0.06365 ± 0.00119
1.1	50	0.2326	20.462 ± 0.035	0.06419 ± 0.00121
1.1	50	0.2413	20.805 ± 0.040	0.06428 ± 0.00146
1.1	50	0.2500	21.155 ± 0.031	0.06374 ± 0.00118
1.1	70	0.0848	14.011 ± 0.100	0.06514 ± 0.00044
1.1	70	0.0935	15.935 ± 0.057	0.06454 ± 0.00032
1.1	70	0.1022	17.356 ± 0.076	0.06478 ± 0.00053
1.1	70	0.1109	18.596 ± 0.036	0.06488 ± 0.00029
1.1	70	0.1196	19.838 ± 0.053	0.06360 ± 0.00050
1.1	70	0.1283	20.914 ± 0.047	0.06257 ± 0.00050
1.1	70	0.1370	21.776 ± 0.039	0.06283 ± 0.00045
1.1	70	0.1457	22.609 ± 0.040	0.06266 ± 0.00052
1.1	70	0.1544	23.370 ± 0.041	0.06269 ± 0.00058
1.1	70	0.1631	24.111 ± 0.043	0.06232 ± 0.00065
1.1	70	0.1718	24.728 ± 0.031	0.06325 ± 0.00050
1.1	70	0.1804	25.456 ± 0.037	0.06179 ± 0.00064
1.1	70	0.1891	26.058 ± 0.039	0.06188 ± 0.00073
1.1	70	0.1978	26.618 ± 0.024	0.06228 ± 0.00048
1.1	70	0.2065	27.170 ± 0.029	0.06239 ± 0.00061
1.1	70	0.2152	27.713 ± 0.027	0.06223 ± 0.00060
1.1	70	0.2239	28.223 ± 0.025	0.06235 ± 0.00059
1.1	70	0.2326	28.727 ± 0.028	0.06220 ± 0.00070
1.1	70	0.2413	29.208 ± 0.026	0.06218 ± 0.00069
1.1	70	0.2500	29.664 ± 0.038	0.06241 ± 0.00107

References

- [1] K. Yasuoka, M. Matsumoto, Molecular dynamics of homogeneous nucleation in the vapor phase. I. Lennard-Jones fluid, *The Journal of Chemical Physics* 109 (19) (1998) 8451–8462. doi:10.1063/1.477509.

- [2] S. Auer, D. Frenkel, Prediction of absolute crystal-nucleation rate in hard-sphere colloids, *Nature* 409 (6823) (2001) 1020–1023. doi:10.1038/35059035.
- [3] G. Chkonia, J. Wölk, R. Strey, J. Wedekind, D. Reguera, Evaluating nucleation rates in direct simulations, *The Journal of Chemical Physics* 130 (6) (2009) 064505. doi:10.1063/1.3072794.
- [4] K. K. Tanaka, K. Kawamura, H. Tanaka, K. Nakazawa, Tests of the homogeneous nucleation theory with molecular-dynamics simulations. I. Lennard-Jones molecules, *The Journal of Chemical Physics* 122 (18) (2005) 184514. doi:10.1063/1.1896345.
- [5] D. I. Zhukhovitskii, Enhancement of the droplet nucleation in a dense supersaturated Lennard-Jones vapor, *The Journal of Chemical Physics* 144 (18) (2016) 184701. doi:10.1063/1.4948436.
- [6] K. Laasonen, S. Wonczak, R. Strey, A. Laaksonen, Molecular dynamics simulations of gas–liquid nucleation of Lennard-Jones fluid, *The Journal of Chemical Physics* 113 (21) (2000) 9741–9747. doi:10.1063/1.1322082.
- [7] J. Wedekind, G. Chkonia, J. Wölk, R. Strey, D. Reguera, Crossover from nucleation to spinodal decomposition in a condensing vapor, *The Journal of Chemical Physics* 131 (11) (2009) 114506. doi:10.1063/1.3204448.
- [8] J. Diemand, R. Angélil, K. K. Tanaka, H. Tanaka, Large scale molecular dynamics simulations of homogeneous nucleation, *The Journal of Chemical Physics* 139 (7) (2013) 074309. doi:10.1063/1.4818639.
- [9] K. K. Tanaka, J. Diemand, R. Angélil, H. Tanaka, Free energy of cluster formation and a new scaling relation for the nucleation rate, *The Journal of Chemical Physics* 140 (19) (2014) 194310. doi:10.1063/1.4875803.
- [10] J. Diemand, R. Angélil, K. K. Tanaka, H. Tanaka, Direct simulations of homogeneous bubble nucleation: Agreement with classical nucleation theory and no local hot spots, *Physical Review E* 90 (2014) 052407. doi:10.1103/PhysRevE.90.052407.

- [11] P. Hänggi, P. Talkner, M. Borkovec, Reaction-rate theory: fifty years after kramers, *Reviews of Modern Physics* 62 (1990) 251–341. doi:10.1103/RevModPhys.62.251.
- [12] R. Angélil, J. Diemand, K. K. Tanaka, H. Tanaka, Properties of liquid clusters in large-scale molecular dynamics nucleation simulations, *The Journal of Chemical Physics* 140 (7) (2014) 074303. doi:10.1063/1.4865256.
- [13] D. Kashchiev, On the relation between nucleation work, nucleus size, and nucleation rate, *The Journal of Chemical Physics* 76 (10) (1982) 5098–5102. doi:10.1063/1.442808.
- [14] S. Izrailev, S. Stepaniants, B. Isralewitz, D. Kosztin, H. Lu, F. Molnar, W. Wriggers, K. Schulten, Steered molecular dynamics, in: Computational Molecular Dynamics: Challenges, Methods, Ideas, Springer, Berlin, Germany, 1999, pp. 39–65. doi:10.1007/978-3-642-58360-5_2.
- [15] C. Dellago, P. G. Bolhuis, P. L. Geissler, Transition path sampling, in: Advances in Chemical Physics, John Wiley & Sons, Inc., Hoboken, NJ, USA, 2002, pp. 1–78. doi:10.1002/0471231509.ch1.
- [16] P. G. Bolhuis, D. Chandler, C. Dellago, P. L. Geissler, Transition path sampling: Throwing ropes over rough mountain passes, in the dark, *Annual Review of Physical Chemistry* (Volume 53, 2002) (2002) 291–318. doi:10.1146/annurev.physchem.53.082301.113146.
- [17] B. Peters, B. L. Trout, Obtaining reaction coordinates by likelihood maximization, *Journal of Chemical Physics* 125 (5) (2006) 054108. doi:10.1063/1.2234477.
- [18] R. J. Allen, C. Valeriani, P. R. t. Wolde, Forward flux sampling for rare event simulations, *Journal of Physics: Condensed Matter* 21 (46) (2009) 463102. doi:10.1088/0953-8984/21/46/463102.
- [19] J. Kästner, Umbrella sampling, *WIREs Comput. Mol. Sci.* 1 (6) (2011) 932–942. doi:10.1002/wcms.66.

- [20] C. Hartmann, R. Banisch, M. Sarich, T. Badowski, C. Schütte, Characterization of rare events in molecular dynamics, *Entropy* 16 (1) (2013) 350–376. doi:10.3390/e16010350.
- [21] J. S. Patel, A. Berteotti, S. Ronisvalle, W. Rocchia, A. Cavalli, Steered molecular dynamics simulations for studying protein–ligand interaction in cyclin–dependent kinase 5, *Journal of Chemical Information and Modeling* 54 (2) (2014) 470–480. doi:10.1021/ci4003574.
- [22] J. Comer, J. C. Gumbart, J. Hénin, T. Lelièvre, A. Pohorille, C. Chipot, The Adaptive Biasing Force Method: Everything You Always Wanted To Know but Were Afraid To Ask, *Journal of Physical Chemistry B* 119 (3) (2015) 1129–1151. doi:10.1021/jp506633n.
- [23] R. C. Bernardi, M. C. R. Melo, K. Schulten, Enhanced sampling techniques in molecular dynamics simulations of biological systems, *Biochimica et Biophysica Acta (BBA) - General Subjects* 1850 (5) (2015) 872–877. doi:10.1016/j.bbagen.2014.10.019.
- [24] R. G. Mullen, J.-E. Shea, B. Peters, Easy transition path sampling methods: Flexible-length aimless shooting and permutation shooting, *Journal of Chemical Theory and Computation* 11 (6) (2015) 2421–2428. doi:10.1021/acs.jctc.5b00032.
- [25] G. Bussi, A. Laio, Using metadynamics to explore complex free-energy landscapes, *Nature Reviews Physics* 2 (2020) 200–212. doi:10.1038/s42254-020-0153-0.
- [26] U. Raucci, V. Rizzi, M. Parrinello, Discover, sample, and refine: Exploring chemistry with enhanced sampling techniques, *Journal of Physical Chemistry Letters* 13 (6) (2022) 1424–1430. doi:10.1021/acs.jpcllett.1c03993.
- [27] T. Burgin, S. Ellis, H. B. Mayes, ATESA: An automated aimless shooting workflow, *Journal of Chemical Theory and Computation* 19 (1) (2023) 235–244. doi:10.1021/acs.jctc.2c00543.
- [28] W. Gispen, J. R. Espinosa, E. Sanz, C. Vega, M. Dijkstra, Variational umbrella seeding for calculating nucleation barriers, *The Journal of Chemical Physics* 160 (17) (2024) 174501. doi:10.1063/5.0204540.

- [29] J. R. Espinosa, C. Vega, C. Valeriani, E. Sanz, Seeding approach to crystal nucleation, *The Journal of Chemical Physics* 144 (3) (2016) 034501. doi:10.1063/1.4939641.
- [30] P. Rosales-Pelaez, I. Sanchez-Burgos, C. Valeriani, C. Vega, E. Sanz, Seeding approach to nucleation in the NVT ensemble: The case of bubble cavitation in overstretched Lennard-Jones fluids, *Physical Review E* 101 (2020) 022611. doi:10.1103/PhysRevE.101.022611.
- [31] I. Sanchez-Burgos, P. M. de Higes, P. Rosales-Pelaez, C. Vega, E. Sanz, Equivalence between condensation and boiling in a Lennard-Jones fluid, *Physical Review E* 102 (2020) 062609. doi:10.1103/PhysRevE.102.062609.
- [32] P. Rosales-Pelaez, M. I. Garcia-Cid, C. Valeriani, C. Vega, E. Sanz, Seeding approach to bubble nucleation in superheated Lennard-Jones fluids, *Physical Review E* 100 (2019) 052609. doi:10.1103/PhysRevE.100.052609.
- [33] R. Becker, W. Döring, Kinetische behandlung der keimbildung in übersättigten dämpfen, *Annalen der Physik* 416 (8) (1935) 719–752. doi:10.1002/andp.19354160806.
- [34] M. Volmer, Kinetik der phasenbildung, Steinkopff, Dresden/Leipzig, 1939. doi:10.1002/bbpc.19400460512.
- [35] J. Zeldovich, Theory of nucleation and condensation, *Soviet Journal of Experimental and Theoretical Physics* 12 (1942) 525.
- [36] Y. Frenkel, Kinetic theory of liquids, Oxford University Press, Oxford, 1946. doi:10.1021/j150454a025.
- [37] D. Turnbull, J. C. Fisher, Rate of nucleation in condensed systems, *The Journal of Chemical Physics* 17 (1) (1949) 71–73. doi:10.1063/1.1747055.
- [38] J. Feder, K. C. Russell, J. Lothe, G. M. Pound, Homogeneous nucleation and growth of droplets in vapours, *Advances in Physics* 15 (57) (1966) 111–178. doi:10.1080/00018736600101264.

- [39] P. Montero de Higes, J. R. Espinosa, V. Bianco, E. Sanz, C. Vega, Interfacial free energy and Tolman length of curved liquid–solid interfaces from equilibrium studies, *The Journal of Physical Chemistry C* 124 (16) (2020) 8795–8805. doi:10.1021/acs.jpcc.0c00816.
- [40] P. Montero de Higes, C. Vega, On the thermodynamics of curved interfaces and the nucleation of hard spheres in a finite system, *The Journal of Chemical Physics* 156 (1) (2022) 014505. doi:10.1063/5.0072175.
- [41] C. P. Lamas, E. Sanz, C. Vega, E. G. Noya, Estimation of bubble cavitation rates in a symmetrical Lennard-Jones mixture by NVT seeding simulations, *The Journal of Chemical Physics* 158 (12) (2023) 124109. doi:10.1063/5.0142109.
- [42] J. W. P. Schmelzer, G. S. Boltachev, V. G. Baidakov, Classical and generalized Gibbs’ approaches and the work of critical cluster formation in nucleation theory, *The Journal of Chemical Physics* 124 (19) (2006) 194503. doi:10.1063/1.2196412.
- [43] A. S. Abyzov, J. W. P. Schmelzer, Nucleation versus spinodal decomposition in confined binary solutions, *The Journal of Chemical Physics* 127 (11) (2007) 114504. doi:10.1063/1.2774989.
- [44] J. W. P. Schmelzer, A. S. Abyzov, Thermodynamic analysis of nucleation in confined space: Generalized Gibbs approach, *The Journal of Chemical Physics* 134 (5) (2011) 054511. doi:10.1063/1.3548870.
- [45] D. Reguera, R. K. Bowles, Y. Djikaev, H. Reiss, Phase transitions in systems small enough to be clusters, *The Journal of Chemical Physics* 118 (1) (2003) 340–353. doi:10.1063/1.1524192.
- [46] Ø. Wilhelmsen, D. Bedeaux, S. Kjelstrup, D. Reguera, Communication: Superstabilization of fluids in nanocontainers, *The Journal of Chemical Physics* 141 (7) (2014) 071103. doi:10.1063/1.4893701.
- [47] Ø. Wilhelmsen, D. Reguera, Evaluation of finite-size effects in cavitation and droplet formation, *The Journal of Chemical Physics* 142 (6) (2015) 064703. doi:10.1063/1.4907367.
- [48] T. Philippe, Nucleation and superstabilization in small systems, *Physical Review E* 96 (2017) 032802. doi:10.1103/PhysRevE.96.032802.

- [49] J. K. Johnson, J. A. Zollweg, K. E. Gubbins, The Lennard-Jones equation of state revisited, *Molecular Physics* 78 (3) (1993) 591–618. doi:[10.1080/00268979300100411](https://doi.org/10.1080/00268979300100411).
- [50] J. Kolafa, I. Nezbeda, The Lennard-Jones fluid: an accurate analytic and theoretically-based equation of state, *Fluid Phase Equilibria* 100 (1994) 1–34. doi:[10.1016/0378-3812\(94\)80001-4](https://doi.org/10.1016/0378-3812(94)80001-4).
- [51] S. Stephan, J. Staubach, H. Hasse, Review and comparison of equations of state for the Lennard-Jones fluid, *Fluid Phase Equilibria* 523 (2020) 112772. doi:[10.1016/j.fluid.2020.112772](https://doi.org/10.1016/j.fluid.2020.112772).
- [52] A. P. Thompson, H. M. Aktulga, R. Berger, D. S. Bolintineanu, W. M. Brown, P. S. Crozier, P. J. in 't Veld, A. Kohlmeyer, S. G. Moore, T. D. Nguyen, R. Shan, M. J. Stevens, J. Tranchida, C. Trott, S. J. Plimpton, LAMMPS - a flexible simulation tool for particle-based materials modeling at the atomic, meso, and continuum scales, *Computer Physics Communications* 271 (2022) 108171. doi:[10.1016/j.cpc.2021.108171](https://doi.org/10.1016/j.cpc.2021.108171).
- [53] T. D. Nguyen, GPU-accelerated tersoff potentials for massively parallel Molecular Dynamics simulations, *Computer Physics Communications* 212 (2017) 113–122. doi:[10.1016/j.cpc.2016.10.020](https://doi.org/10.1016/j.cpc.2016.10.020).
- [54] V. G. Baidakov, S. P. Protsenko, Z. R. Kozlova, The self-diffusion coefficient in stable and metastable states of the Lennard–Jones fluid, *Fluid Phase Equilibria* 305 (2) (2011) 106–113. doi:[10.1016/j.fluid.2011.03.002](https://doi.org/10.1016/j.fluid.2011.03.002).
- [55] V. G. Baidakov, S. P. Protsenko, Z. R. Kozlova, G. G. Chernykh, Metastable extension of the liquid-vapor phase equilibrium curve and surface tension, *The Journal of Chemical Physics* 126 (21) (2007) 214505. doi:[10.1063/1.2734964](https://doi.org/10.1063/1.2734964).
- [56] Ø. Wilhelmsen, D. Bedeaux, S. Kjelstrup, D. Reguera, Thermodynamic stability of nanosized multicomponent bubbles/droplets: The square gradient theory and the capillary approach, *The Journal of Chemical Physics* 140 (2) (2014) 024704. doi:[10.1063/1.4860495](https://doi.org/10.1063/1.4860495).
- [57] J. H. Irving, J. G. Kirkwood, The statistical mechanical theory of transport processes. IV. the equations of hydrodynamics, *The Journal of Chemical Physics* 18 (6) (1950) 817–829. doi:[10.1063/1.1747782](https://doi.org/10.1063/1.1747782).

- [58] A. Stukowski, Visualization and analysis of atomistic simulation data with ovito—the open visualization tool, *Modelling and Simulation in Materials Science and Engineering* 18 (1) (2010). doi:10.1088/0965-0393/18/1/015012.
- [59] J. F. Lutsko, Theoretical description of the nucleation of vapor bubbles in a superheated fluid, *EPL (Europhysics Letters)* 83 (4) (2008) 46007. doi:10.1209/0295-5075/83/46007.
- [60] J. F. Lutsko, G. Nicolis, The effect of the range of interaction on the phase diagram of a globular protein, *The Journal of Chemical Physics* 122 (24) (2005) 244907. doi:10.1063/1.1943987.
- [61] B. Peng, Y.-X. Yu, A density functional theory for Lennard-Jones fluids in cylindrical pores and its applications to adsorption of Nitrogen on MCM-41 materials, *Langmuir* 24 (21) (2008) 12431–12439, publisher: American Chemical Society. doi:10.1021/la8024099.